Trans. JSASS Aerospace Tech. Japan
Vol. 19, No. 3, pp. 415-423, 2021
DOI: 10.2322/tastj.19.415

Numerical Study on Combustor Flow-Path Design for a Scramjet Flight Experiment

By Masahiro TAKAHASHI,[1)] Sadatake TOMIOKA,[1)] Masatoshi KODERA,[1)] Kan KOBAYASHI,[1)] Susumu HASEGAWA,[1)] Taro SHIMIZU,[2)] Junya AONO,[3)] and Toshihiko MUNAKATA[4)]

[1)]*Research Unit IV, Research and Development Directorate, JAXA, Kakuda, Japan*
[2)]*Research Unit III, Research and Development Directorate, JAXA, Sagamihara, Japan*
[3)]*Research Center of Computational Mechanics, Inc., Tokyo, Japan*
[4)]*Hitachi Solutions East Japan, Sendai, Japan*

(Received July 12th, 2019)

A flight-ground test comparison program is undergoing at JAXA to reveal so-called facility effects on hypersonic aerodynamics and combustion phenomena. The flight vehicle will mount a combustor duct along its centerline, with so-called alligator type inlet with side-spillage to attain good starting characteristics. The incoming flow condition was estimated with 3D-CFD, and one-dimensional chemical kinetic calculation was conducted to settle design guideline of combustor which could enhance so-called vitiation effects on combustion. The design guideline was further evaluated by 3D-CFD with fine chemical reaction model, showing possible difference in combustion efficiency and resulting pressure level.

Key Words: Supersonic Combustion, CFD, Flight Experiment, Ground Testing

Nomenclature

M	:	Mach number
Sc_T	:	turbulent Schmidt number
t	:	time
X	:	position

1. Introduction

To realize a hypersonic flight system, research and development of hypersonic air-breathing propulsion systems such as a scramjet has been actively conducted in various countries of the world. Both ground tests and CFD play important roles for its development. By making the best use of these, it is expected to reduce the number of the flight tests and to reduce the development costs.

To apply the combustion test data to the actual engine design, however, it is necessary to consider the influence of the flow characteristics, which the ground test facility produces, on the combustion test data, that is, the facility dependence. For example, to reproduce the high-speed airflow corresponding to the scramjet operating conditions in the wind tunnel, it is necessary to heat up an airflow to raise the total temperature. JAXA has built a large blow-down-type wind tunnel for the engine test at the Kakuda Space Center, named as Ramjet Engine Test Facility (RJTF).[1)] The RJTF has capability to reproduce flow conditions for the hypersonic air-breathing engine tests, which correspond to the flight Mach number of 4, 6, and 8. The engine model of up to 3 meter-long can be tested. The RJTF has two different types of the airflow heating devices. One is a storage air heater (SAH) and the other is a vitiation air heater (VAH). The SAH heats the airflow by heat exchange with the heated bricks. The VAH raises the total temperature of the airflow by adding hydrogen and oxygen to the airflow and burning them. The oxygen concentration in the VAH test flow is kept at 21% in mole although water vapor is introduced to the test flow. The unique capability of the RJTF is that both the SAH and VAH can reproduce the test flow corresponding to Mach 6 flight. This allows us to examine the difference of the combustion test results between the SAH and VAH modes. It has been shown in the past work that the engine test results showed some differences depending on the airflow heating method.[2)] It was considered due to the influence of water vapor contained in the VAH test flow on combustion. Since only the VAH can produce the test flow condition over Mach 6 flight, the facility dependence phenomena must be clarified. Therefore, JAXA has started five-years research program to understand the influence of the flow turbulence and the difference of the test flow composition between the flight and facility conditions on combustion and to develop the prediction tool which is able to estimate the actual flight data from the facility data. The final goal of the project is set to conduct the flight experiment to obtain the supersonic combustion data in the real flight and to validate the prediction tool by the flight data.[3)]

In the present study, both one-dimensional analysis and 3D-CFD were performed for the supersonic combustor flow to establish the flow-path design guidelines of the combustor model used for the flight experiment. The requirement for the flow-path design was that sizable difference of the wall pressure distribution would be obtained because of the difference in the composition of the engine incoming flow between the flight and facility conditions. The one-dimensional analysis assessed the outline of the

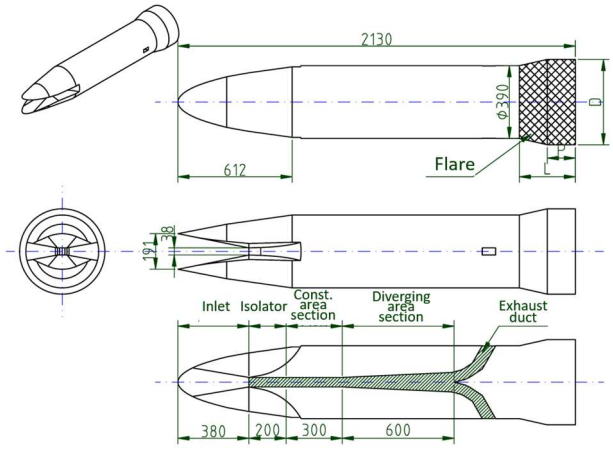

Fig. 1. Schematics of flight experimental vehicle and combustor model.

combustor geometry and the fuel injection condition. The 3D-CFD examined the influence of difference in the composition of the combustor inflow between the flight and facility conditions on combustion and evaluated the suitability of the candidate combustor flow-path geometries to the design requirement.

2. Flight Experimental Vehicle and Supersonic Combustor Model

The schematics of the flight experimental vehicle (FEV) and the supersonic combustor model are shown in Fig. 1.[3] According to the current plan, the FEV will be launched by a sounding rocket. The FEV has an axisymmetric shape, which fits in the nose cone of the launcher. After acceleration by the launcher, the FEV is separated and continues to fly along a ballistic trajectory. The supersonic combustion experiment will be conducted in the descend phase when the FEV is re-accelerated to reach Mach number around 6. The combustor model is symmetrical in the vertical direction and is mounted on the FEV central axis. Considering the inlet start capability at low flight Mach number before the test window starts, a so-called alligator-type inlet was adopted. The inlet height at the entrance is 190.5 mm. The height and the width of the inlet exit are 38.1 mm and 50.8 mm, respectively. The area contraction ratio is 5. The internal flow-path starts from 380 mm downstream of the inlet entrance. It consists of the isolator and the combustor. The isolator is a constant cross-sectional area duct with a rectangular cross-section and its length is 200 mm. The purpose of the isolator is to prevent the flow disturbance caused by high pressure in the combustor from propagating back into the inlet to cause an inlet un-start. The combustor at the early stage of the design study consisted of a 300 mm-long constant cross-sectional area section and a 600 mm-long diverging cross-sectional area section. A primary fuel injector and a flame-holding cavity were installed in the constant area section. The basic idea was that flame-holding would be ensured in the constant area section and the diverging area section would provide moderate pressure-rise accompanying the progress of combustion. It is reasonable to consider that the difference in the wall pressure distribution due to the difference of the freestream composition would increase if large amount of a fuel could be provided while maintaining a supersonic combustion mode. It led us to examine the diverging cross-sectional area combustor without any constant-area section. The details of the flow-path configurations examined will be described at the following section. For these years, use of a hydrocarbon fuel such as a jet fuel has become major for hypersonic air-breathing propulsion systems because of its high thrust density. For the present flight experiment, gaseous ethylene (C_2H_4) is planning to be used since it is one of major components of a thermally-cracked jet fuel and its combustion mechanism is one of the well-understood ones among hydrocarbon fuels.

3. One-Dimensional Assessment on Combustor Geometry and Operation Condition for Vitiation Effects Investigation

3.1. Calculation methods

One-dimensional calculation was conducted to highlight the chemical aspects within the supersonic combustor causing difference in combustion process between the flight condition and the facility condition. The prime target was to set combustor configuration (namely, the divergence angle) and injection conditions (flow rates and locations). In the past study,[2] a one-dimensional chemical kinetic calculation was conducted to evaluate the cause of difference in engine performances in the case with a storage air heater and that with a vitiation (combustion) air heater. In that calculation, a portion of injected fuel was assumed to burn within flame-holding region, and the one-dimensional flow calculation with chemical kinetics was conducted on the mixture of burnt gas, remaining fuel and whole airflow to evaluate the delay in heat release in the streamwise direction, as one-dimensional mixture without this partial combustion could not cause any heat release within the combustor. The same method was used in the present study, the difference being that the fueling was staged in the present case so that the first stage fuel injected within the constant cross-sectional area combustor to burn completely to meet the second stage fuel within the diverging combustor in the present study. As will be described later, the presence of the flame-holding cavity in the present study enhanced the fuel and airflow mixing so that too much heat release caused thermal choking in 3D-CFD, and thus, the second stage fuel was assumed to be separately injected to ensure supersonic, reaction-rate-controlled combustion within the diverging portion. This staged injection will be applied for the real flight model design.

Figure 2 shows the currently expected flight trajectory. Timing is from the onset of the test window. As the test window would be during re-entry and diving phases, flight Mach number was expected to be rather constant, while the dynamic pressure increases rapidly with air density. In the following calculation, the nominal flight condition was set at flight Mach number of 6.2 with dynamic pressure of 62.5 kPa (t=6 sec. in Fig. 2).

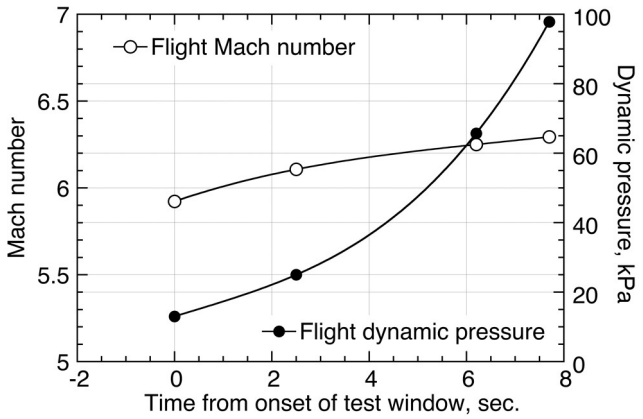

Fig. 2. Time histories of predicted flight Mach number and dynamic pressure within test window.

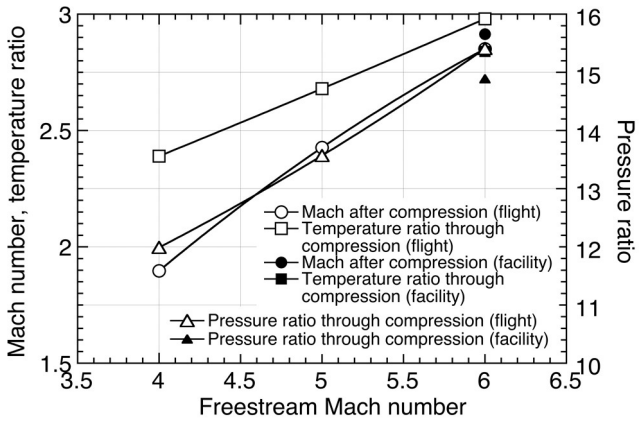

Fig. 3. Variations of Mach number and increments in static pressure and temperature after compression against flight Mach number.

To begin with, the flow states at the entrance of the combustor section should be evaluated. Thus, the inlet performance and the flow states after the compression were evaluated using a 3D-CFD code named FaSTAR.[4] This inlet section was so-called alligator-type, i.e., counter-facing ramp compressions with side-spillage path with contraction ratio of 5. In calculating the flight conditions, specific heat ratio was set to be 1.4, while in calculation of the facility conditions with a vitiation heater, it was set to be 1.38 assuming combustion gas of air, hydrogen and make-up oxygen to keep oxygen mole fraction of 21% in the combustion gas. As for the facility conditions, freestream Mach number, static temperature and static pressure were set to be equal to the flight ones.

Figure 3 shows the variation of the averaged flow states after compression, namely the Mach number, static pressure, and static temperature against flight Mach number. Note that both static pressure and temperature were normalized with freestream values to show increments. To attain averaged values over the cross-section at the exit of the 200-mm-long isolator section (i.e., the entrance of the combustor section), both static pressure and dynamic pressure were area-weighted and static temperature was mass-flow-rate-averaged. Mach number and other states were then calculated based on these values. The 3D-CFD was performed with various Mach

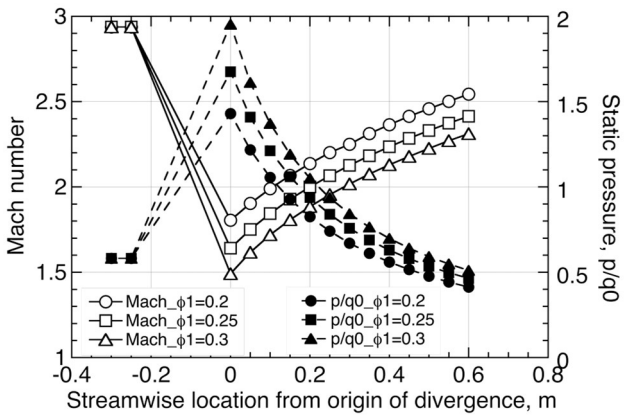

Fig. 4. Predicted Mach number and static pressure distributions with complete combustion of first stage fuel in flight conditions.

Table 1. Comparison of flow states after compression at nominal condition.

	Flight	Facility
Mach number	2.94	3.00
Static pressure, kPa	36.3	35.0
Static temperature, K	679	647
Total temperature, K	1669	1577
Molecular weight, kg/mol	0.0290	0.0271
Specific heat ratio	1.37	1.35

numbers for the flight condition, while it was performed for M=6 condition alone (solid symbol in Fig. 3) for the facility condition, assuming the same gradients on this figure to these for the flight conditions in case with extrapolation. Note that both the pressure and temperature increments were almost linear against freestream Mach number, and though the Mach number shows somehow nonlinear behavior, deviation from linear relation was rather small. As shown in Fig. 2, the flight Mach number would be close to M=6 throughout the test window, so that we expected the extrapolation on the facility flow states to be reasonable.

Table 1 summarizes flow states after the compression at the nominal condition (flight dynamic pressure of 62.5 kPa) for both the flight and facility conditions deduced from Fig. 2. In the facility conditions, the Mach number was slightly high and both static pressure and temperature were slightly low in comparison to those in the flight conditions due to a lower specific heat ratio. Total temperature was lower for the facility case due to high specific heat of water vapor.

The Mach number after the compression was rather low in comparison to referenced values (Reference 5), for example), but this was because of the generation of the detached shock waves at the leading edge of the isolator sidewalls, with traveling shock waves within the isolator duct. The core flow could reach as high as 3.5 at the M=6 flight condition, while the average over cross-section including boundary layer flow was less than 3. In the following one-dimensional calculation, the averaged value was used as input (i.e., flow states at the combustor entrance). So-called skeletal model[6] containing 31 chemical species was used as the chemical mechanism for the air-ethylene combustion and was built in a commercially available one-dimensional reacting flow solver (LSENS, see

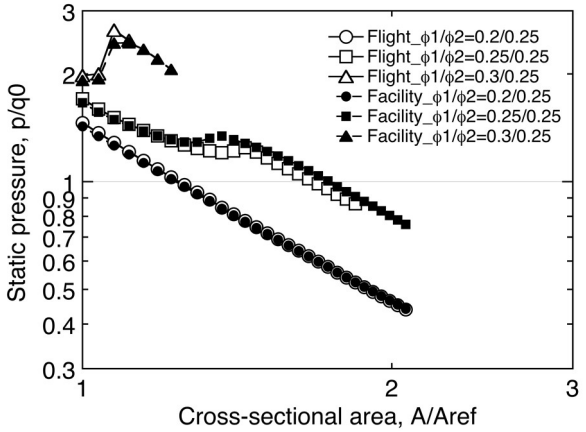

Fig. 5. Predicted static pressure distributions with fixed second stage fuel equivalence ratio of 0.25 at 2 degrees half angle of diverging section.

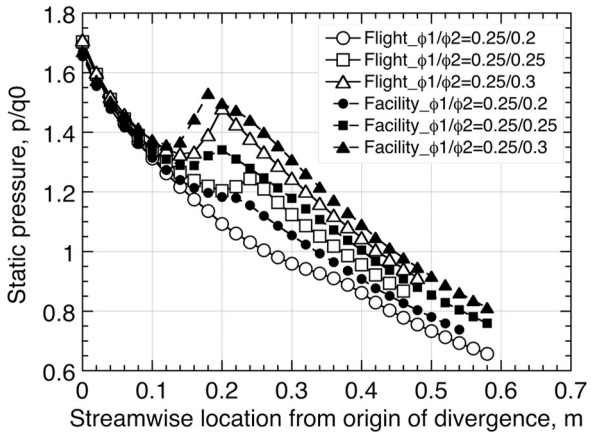

Fig. 6. Predicted static pressure distributions with fixed first stage fuel equivalence ratio of 0.25 at 2 degrees half angle of diverging section.

Ref. 7) for details).

As for the combustor geometry, both the first stage fuel injector and the flame-holding cavity were supposed to be installed within a 300-mm-long constant cross-sectional area combustor section, with the cross-section 50.8 mm in width and 38.1 mm in height. A 600-mm-long diverging cross-sectional area combustor section followed, with its half angle in the height direction 1, 2, and 2.9 degrees. The second stage fuel injector was installed at the origin of the diverging section.

In the one-dimensional calculation, the first stage fuel was assumed to burn completely within the constant section. The combustion gas then mixed with the second stage fuel to form initial mixture for the chemical kinetic calculation within the diverging section. In determining the fuel flow rate, upper limit was set so that the flow would not thermally choke within the duct, because the pressure and temperature recovery within the isolator due to the thermal choking in the downstream combustor would make the chemical reaction less sensitive to the contamination due to the combustion heating process, so that not suitable for the current research perspective. Figure 4 shows the variation of the flow states with complete combustion of the first stage fuel alone, in the flight case. In the case with the first stage equivalence ratio of 0.3, the mean flow decelerated to Mach 1.5. With further increase in the first stage equivalence ratio to 0.4, the mean flow was thermally choked to leave no solution after combustion (mass conservation no longer satisfied). Thus, the maximum first stage equivalence ratio was set to be 0.3.

3.2. Results

Figure 5 compares static pressure distributions for the flight and facility conditions with the fixed second stage equivalence ratio of 0.25, while first stage equivalence ratio was varied. The half angle of the diverging section was 2 degrees in this case. The horizontal axis shows cross-sectional area normalized with that in the constant section, and the vertical axis shows static pressure normalized with the flight dynamic pressure. Note that the figure is on the log-log plot, so that an adiabatic expansion would follow straight line in this figure. With the first stage fuel equivalence ratio of 0.2, heat release by the second stage fuel was not observed in both the flight and facility conditions. With the first stage fuel equivalence ratio of 0.25, on the other hand, heat release and consequent pressure-rise occurred with some delays in the streamwise direction. Note that the delay lengths were different between the flight condition and the facility condition, and the discrepancy between the pressure distributions for both conditions was sizable. With the first stage fuel equivalence ratio of 0.3, heat release from the second stage fuel occurred almost instantly in both conditions, so that the discrepancy was no longer sizable. The above-mentioned results implied that there existed optimal first stage fuel equivalence ratio to highlight the chemical effects on heat release distributions between the flight and facility conditions, and the first stage fuel equivalence ratio was fixed at 0.25 in the following discussion.

Figure 6 compares static pressure distributions for the flight and facility conditions with the fixed first stage equivalence ratio of 0.25, while the second stage equivalence ratio was varied. The half angle of the diverging section was 2 degrees in this case. To highlight the discrepancy in the heat release (pressure-rise) location, the horizontal axis shows the distance in linear scale. With the second stage fuel equivalence ratio of 0.2, the location of the pressure-rise showed clear difference, while the peak value itself was rather small for good detection. With the second stage fuel equivalence ratio of 0.25, the pressure-rise became noticeable, while the discrepancy in the peak pressure location was shortened. The discrepancy was about 50 mm, still sizable with discrete pressure measurement in the flight vehicle. With further increase in the second stage fuel equivalence ratio to 0.3, pressure-rise became further noticeable, while the discrepancy became almost non-detectable. Thus, the second stage fuel equivalence ratio also had optimal value to highlight the chemical effects on heat release distributions between the flight and facility conditions, and both the first and second stage fuel equivalence ratios were set to be 0.25 in the following discussion.

The last effort to highlight the discrepancy of heat release between the flight and facility cases was to change the half angle of the diverging section to either smaller (1 degree) or larger (2.9 degrees). Figure 7 shows the static pressure

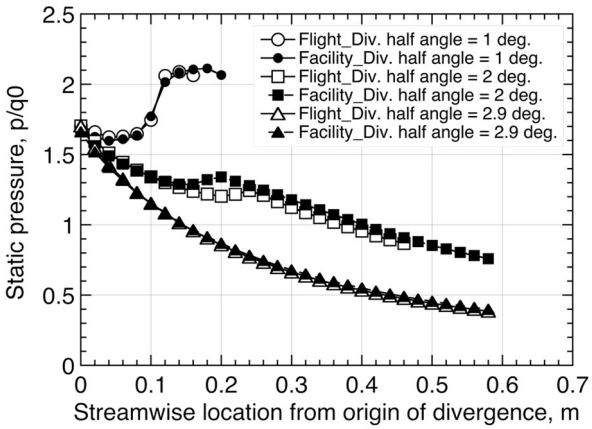

Fig. 7. Predicted static pressure distributions with fixed first- and second-stage fuel equivalence ratios of 0.25 at various half angles of diverging section.

distributions with various half angles, with the fixed first- and second-stage fuel equivalence ratios of 0.25. With the larger half angle, decrease in the static temperature and pressure due to flow expansion enlarge the delay of heat release to cause no sizable pressure-rise within the current combustor ducts. With the smaller half angle, on the other hand, pressure-rise due to heat release became prominent, while the delay lengths of heat release were shortened to make the discrepancy between the flight and facility cases not sizable. Thus, the half angle also had an optimal range. As further effort, several options are at hand such as, 1) increasing both the half angle and the second stage fuel equivalence ratio, or 2) setting the second stage fuel injection point further downstream to lower the static temperature and pressure level for enlarged delay of heat release.

4. Evaluation of Combustor Flow-path Configuration by 3D-CFD

4.1. Numerical method

In this study, 3D-RANS simulations were applied to the supersonic combustor flows by using a JAXA in-house solver LS-FLOW. The LS-FLOW has been originally developed for aerodynamic simulations of an external flow around flying vehicles.[8] The solver used here is an extended version of the LS-FLOW, which can accommodate arbitrary chemical species and chemistry mechanisms.

As mentioned above, the fuel was a gaseous ethylene. Combustion mechanism of hydrocarbon is a complex and large-scale one, to which many chemical species contribute. Therefore, computational time of 3D-CFD increases significantly with ethylene fuel than with hydrogen fuel. On the other hand, an accurate prediction of ethylene combustion process is important for the present study since the main interest is to evaluate the influence of the difference in the freestream composition between the flight and facility conditions on the combustion test results. Considering tradeoff between the accuracy and the computation time, the C_2H_4-air skeletal mechanism of Zambon-Chelliah[6] was adopted for the 3D-CFD. The model is the same one used in the one-dimensional analysis and considers 31 chemical species and 128 elementary reactions.

The details of the numerical procedure were given in Ref. 9). The 3D-CFD was conducted by using the JAXA Supercomputer System (JSS2).

4.2. Evaluation method

Since 3D-CFD using the skeletal mechanism requires long computational time, the computational domain was limited to be the flow-path in the isolator and the combustor. The upstream boundary was set at 20 mm downstream from the isolator entrance and the cross-sectional distributions of the major variables obtained from other 3D-CFD for the upstream flows were given as the inflow condition. The inflow condition of the flight condition was obtained by a non-reacting 3D-CFD around the forebody of the FEV, which included the inlet and the internal flow-path of the isolator. The representative flight test conditions were the flight Mach number of 6.1 and the dynamic pressure of 62.5 kPa. In the facility case, a so-called direct-connect setup, which has been the most often used setup for the fundamental research of the combustors, was targeted in the present study. For this setup, the flow conditions of the airflow after the inlet compression are simulated by a nozzle flow of a VAH supersonic wind tunnel. The isolator is connected directly to the facility nozzle exit and the whole nozzle flow is captured into the isolator flow-path. The inflow conditions for the combustor CFD were computed by another CFD of a reacting flow in the VAH facility nozzle and the isolator of the test model. Here, the freestream Mach number, static temperature, and static pressure of the facility nozzle flow were set to be the same as those after inlet compression in case of the flight condition. Note that, according to the VAH nozzle flow CFD, the facility flow would contain water vaper of 15% by mass and very small amount of radical species.

4.3. Combustor flow-path configuration

In this report, among the combustor flow-path candidates evaluated so far, the results of the flow-path, with which the most distinguish difference in the combustor pressure distribution appeared between the flight and facility conditions and high combustor performance was also achieved, are shown.

The flow-path configuration is shown in Fig. 8. This configuration was derived by modifying the one used for a scramjet flight experiment HIFiRE Flight 2,[10] which has been conducted by the United States and Australia. At early stage of this study, the combustor configuration with the 300 mm-long constant cross-sectional area section followed by the

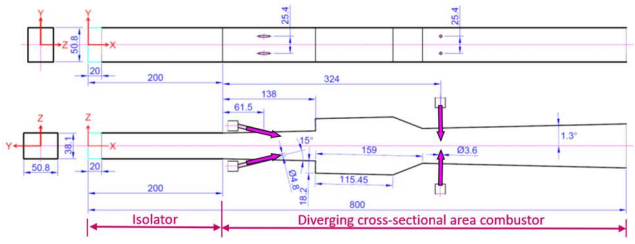

Fig. 8. Combustor flow-path configuration.

diverging cross-sectional area section has been evaluated. A parallel ramp injector with injection angle of 10 degree to the combustor wall and a flame-holding cavity were mounted in the constant-area section. The numerical results, however, showed that transition to subsonic-combustion mode occurred with all the configurations when ethylene fuel was injected at an equivalence ratio of 0.5. In this design study, supersonic-combustion mode operation was preferred because of rather simple flow structure in the combustor, lower heat load to the combustor wall and less risk of transition to catastrophic inlet un-start situation during the flight test comparing with the subsonic-combustion mode. The supersonic-combustion mode could be achieved by lowering the equivalence ratio down to 0.3 and the design evaluation was attempted. In this case, however, the combustion pressure-rise became small and no sizable difference in the combustion pressure between the flight and facility conditions could be achieved. As shown by the one-dimensional assessment in the previous section, there would be appropriate amount of the fuel, which enables to obtain sizable difference of the combustor pressure distribution between the flight and facility conditions. Therefore, we decided to modify the combustor flow-path geometry so that C_2H_4 fuel as much as the total equivalence ratio of 0.5 could be supplied while maintaining the supersonic-combustion mode. According to Ref. 11), the HIFiRE 2 combustor has achieved high performance and favorable characteristic for our design study. A large amount of C_2H_4 / CH_4 mixture fuel, which corresponded to the total equivalence ratio of unity, was supplied and the combustion efficiency as high as 0.7 or higher was achieved while the supersonic-combustion mode was maintained at the Mach 8 flight condition. Since both the operating condition and the design requirements of the combustor were different between the HIFiRE 2 and our flight experiment, parametric study for the combustor design was conducted by the 3D-CFD to tune-up the geometry. The baseline configuration was 1.5 times scale-up of the HIFiRE 2 combustor since the combustor height was 25.4 mm for the HIFiRE 2 and 38.1 mm for our combustor. Several combustor configurations with different cavity shapes and different positions and numbers of the injection holes were compared. The combustor flow-path configuration shown in Fig. 8 is one of the candidates selected from the parametric study. The basic configuration is the same as the HIFiRE 2 combustor. It is a two-dimensional diverging area combustor with a rectangular cross-section and is symmetric in the height direction. The half expansion angle of the top and bottom walls is 1.3 degree. Large flame-holding cavities are installed on both the top and bottom walls. Staged fuel injection is employed. The first stage fuel injector is installed upstream of the cavity. The fuel is injected obliquely with the injection angle of 15 degree to the combustor wall. The second stage fuel injector is installed downstream of the cavity. The fuel is injected perpendicular to the combustor wall. As for the change from the similar geometry of the HIFiRE 2 combustor, the cavity depth was made relatively shallow by 30%.

4.4. Results

The computational grid is shown in Fig. 9. Considering

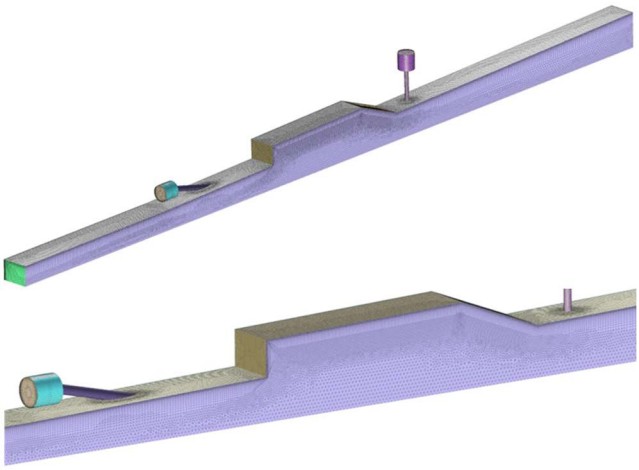

Fig. 9. Computational grid.

symmetry of the flow-path geometry in both the height and spanwise directions, only a flow in the quarter space of the flow-path was computed and the symmetrical boundary condition was applied at the center plane in the both the height and spanwise directions. The total number of the elements was about 3.3 million. The minimum grid size near the wall was 10 micrometers. As mentioned above, cross-sectional distributions of major variables, which were predicted by other CFD for either the flight condition or the facility condition, were given as the inflow condition at the upstream boundary. Non-slip and isothermal walls were assumed as the wall boundary condition. The wall temperature was fixed at 700 K. The fuel is gaseous ethylene. Both a short pipe and a fuel manifold were attached to each injector hole. At the inflow boundary of the fuel manifold, a fuel mass flow rate and a static temperature were given. The equivalence ratios of both the first and second stage injectors were fixed at 0.25 and 0.25 and the total equivalence ratio was 0.5. The previous work showed that the turbulent Schmidt number (Sc_T), which changes contribution of turbulent diffusion to fuel-air mixing with smaller number corresponding to further mixing enhancement, strongly affected the combustor CFD results and that the CFD with Sc_T=0.3 resulted in better agreement with the experimental results than that with Sc_T=0.9.[9] To examine its influence in the present case, CFD with both Sc_T=0.3 and Sc_T=0.9 were conducted.

Figure 10 shows contour plots of major quantities in the vertical plane which includes the fuel injection holes. Each figure shows, from the top, the static temperature, the Mach number, and the mass fraction of H_2O and CO_2 produced by the combustion of C_2H_4 fuel. The amount of H_2O in the case of the facility condition is a value obtained by subtracting the amount of H_2O originally contained in the VAH facility nozzle flow from the total amount of H_2O. A black solid line in each figure shows a sonic line. The upper and lower figures of each quantity show the result of the flight condition and that of the facility condition, respectively. The results with Sc_T=0.3 are shown. There was no significant difference in the combustor flow structures between the flight and facility conditions. In both cases, the fuel was burning well in the cavity and the supersonic freestream flowed through the

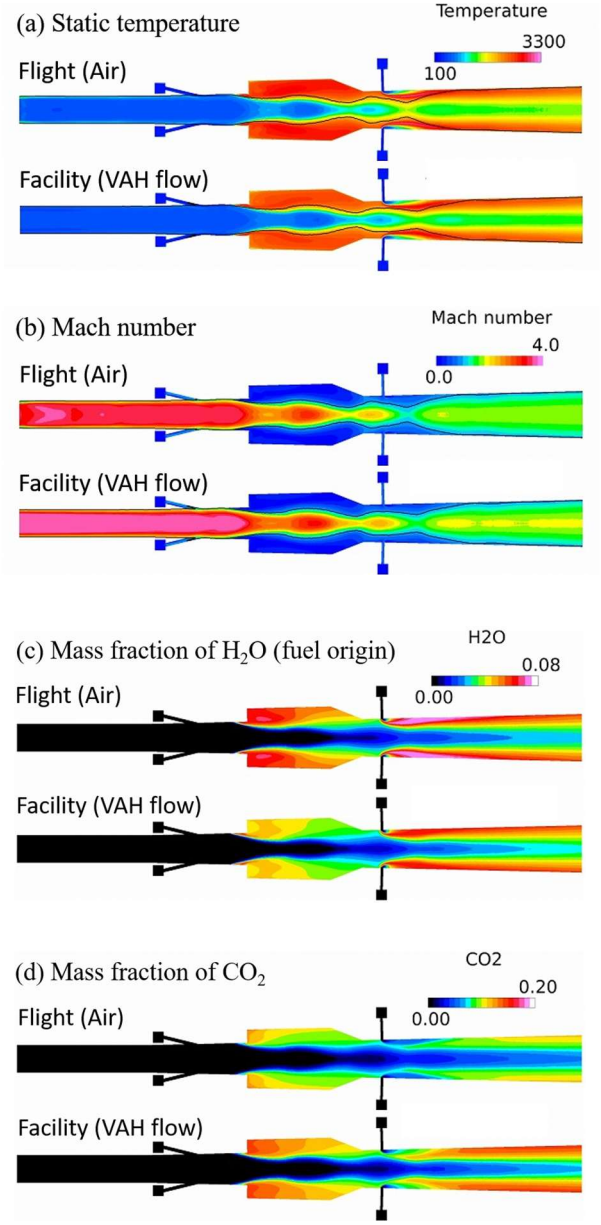

Fig. 10. Contour plots in vertical cross-section including fuel injection ports; (a) Static temperature (b) Mach number (c) Mass fraction of H_2O produced from fuel (d) Mass fraction of CO_2. Fuel equivalence ratio of first- and second-stage injectors were 0.25 and 0.25. Turbulent Schmidt number Sc_T was 0.3.

central area. A part of the high temperature region spread along the wall beyond upstream corner of the cavity. That is, pressure-rise due to combustion in the cavity caused boundary layer separation upstream of the cavity. In the supersonic freestream, the separation shock waves were formed and repeated incidence and reflection between the central plane of symmetry and the shear layer at the freestream outer edge. As a result, the supersonic freestream repeated expansion and contraction in the combustor height direction. The supersonic freestream became the narrowest and the Mach number also became the lowest at a position slightly downstream of the second stage fuel injector location. After that, the freestream rapidly spread in the height direction and the Mach number

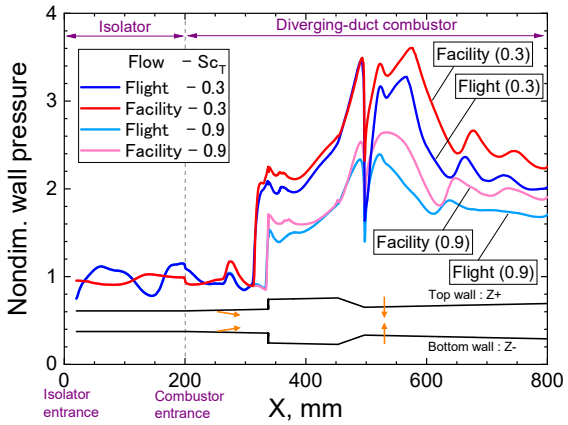

Fig. 11. Comparison of wall pressure distribution normalized by value averaged from X=150 mm to X=200 mm; Fuel equivalence ratio of first- and second-stage injectors were 0.25 and 0.25.

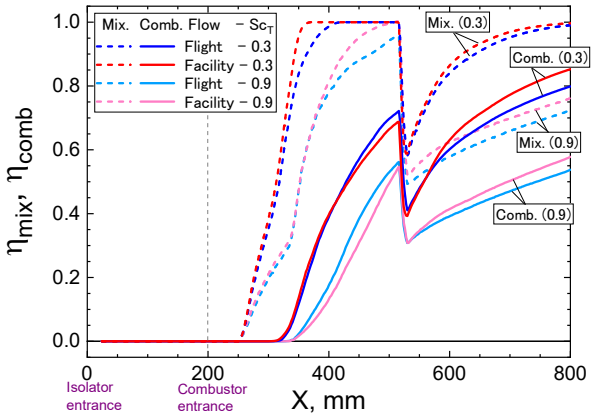

Fig. 12. Distribution of mixing efficiency and combustion heat release efficiency; Fuel equivalence ratio of first- and second-stage injectors were 0.25 and 0.25.

also increased. On the other hand, the mass fraction of H_2O and CO_2 increased near the wall downstream of the second stage injector. It means that the secondary fuel was burning. The remarkable difference is that H_2O production was active in the case of the flight condition while CO_2 production was active in the case of the facility condition. The reason of this will be discussed later.

Figure 11 shows comparison of the wall pressure distribution along the center line of the top wall between the flight and facility conditions. Both the results with Sc_T =0.3 and those with Sc_T=0.9 are shown. The wall pressure shown here was the value normalized by the wall pressure averaged from X=150 mm to X=200 mm in the isolator section. In the flame-holding cavity, where combustion was active, and its downstream region, the wall pressure of the facility condition was higher than that of the flight condition. Clear difference was observed at the downstream region of the second stage injector no matter with Sc_T=0.3 and Sc_T=0.9.

Figure 12 shows the variation of the mixing efficiency and the combustion efficiency along the combustor axis. The combustion efficiency was defined as the ratio of the obtained combustion heat release to the ideal heat release assuming that

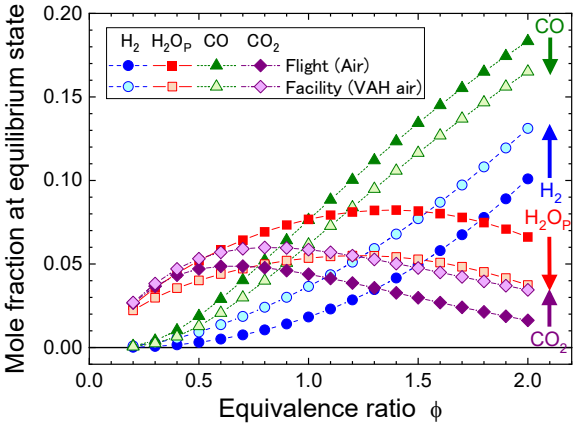

Fig. 13. Equilibrium composition of C_2H_4 combustion in mole fraction; initial pressure was 40 kPa, initial temperature was 1700 K, constant-volume combustion was assumed.

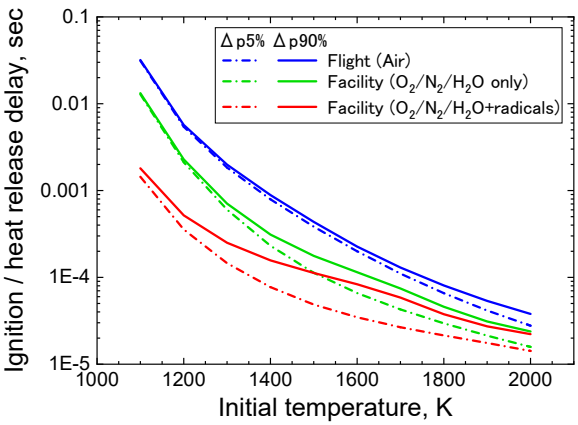

Fig. 14. Ignition delay time and combustion heat release completion time of C_2H_4 combustion; initial pressure was 40 kPa, equivalence ratio was unity, constant-volume combustion was assumed.

all the fuel changes to H_2O and CO_2. The sudden drop of both the mixing efficiency and the combustion efficiency near X=520 mm was due to the second stage fuel injection. The combustion efficiency at the exit of the combustor was as high as 80% in the flight condition and 85% in the facility condition. Both the mixing efficiency and the combustion efficiency of the facility condition were higher than those of the flight condition. It is noted that the difference in the mixing efficiency was marginal but the difference in the combustion efficiency was as large as 5%. This suggested that the difference in the combustion pressure between the flight and facility conditions seen in Fig. 11 was likely due to the difference in the combustion efficiency.

4.5. Discussion

In this section, the influence of the difference in the freestream composition between the flight and facility conditions on combustion is discussed.

First, as shown in Fig. 10, the CFD predicted that H_2O production was active in the case of the flight condition while CO_2 production was active in the case of the facility condition. The reason would be difference in equilibrium state of the fuel combustion between the flight and facility conditions due to H_2O contained in the combustion-heated airflow of the facility case. Figure 13 shows the equilibrium composition of C_2H_4 combustion for both the flight and facility conditions. The initial conditions of unburned gas mixture were static pressure of 40 kPa and static temperature of 1700 K, being those simulated flow conditions in the flame-holding cavity. The equilibrium composition was calculated by assuming constant volume process. The equivalence ratio ranged from 0.2 to 2.0. Although the total amount of H_2O was larger, the amount of H_2O produced by the fuel combustion was smaller and, instead, more CO_2 was produced in the case of the facility condition than in the case of the flight condition. As combustion progresses and the static temperature rises, each elementary reaction, and eventually, whole combustion state approaches to the equilibrium states. In the flame-holding cavity, the gas temperature was high, and the combustion gas composition was likely influenced by the equilibrium characteristics. As the equivalence ratio increased to become more than unity, the amount of CO and H_2 increased while the amount of H_2O and CO_2 decreased because amount of O_2 was in short. The difference of equilibrium composition between the flight and facility conditions remained clearly or even increased as the equivalence ratio increased.

Next, the difference in the combustion efficiency between the flight and facility conditions is discussed. From Fig. 10, there was no significant difference in the flow-field structure between the flight and facility conditions. As shown in Fig. 12, the mixing efficiency was also similar. In the meantime, the combustion efficiency was lower than the mixing efficiency for both the flight and facility conditions, meaning that the combustion state did not reach an equilibrium. From those observation, it was considered that the difference in the combustion efficiency was due to the difference in the degree of progress of the chemical reaction. Figure 14 shows the ignition-delay time and the combustion heat release time of C_2H_4 combustion with respect to the initial temperature calculated by using CHEMKIN software. The results of both the flight and facility conditions are shown. As for the initial condition of the 0-dimensional analysis assuming a constant-volume combustion, the pressure was 40 kPa, the equivalence ratio was unity, and the initial temperature was varied. The ignition-delay time was defined as a time when the pressure-rise equivalent to 5% of the final combustion pressure-rise was reached while the heat release time was a time for the 90% pressure-rise. As for the facility conditions, two compositions of the oxidizer were examined. One was the composition of the VAH nozzle flow predicted by CFD with H_2-air chemistry, which contained the combustion-heating product of H_2O and small amount of radical species, and the other was those without the radicals. The ignition-delay time of the facility condition including all radicals was much shorter than that of the flight condition, and that of the facility condition without radicals was in between. The order of the heat release time was the same as that of the ignition-delay. When H_2O or radicals produced by the combustion-heating of the airflow are contained in air, both the ignition-delay and heat release times tend to become shorter than those with pure air. That is, also for the combustion process in the combustor,

ignition and heat release are likely faster in the facility condition than in the flight condition. In the one-dimensional analysis of the previous section, the heat release delay was shorter in the facility condition, and it was for this reason that the combustion pressure-rise occurred at further upstream position. From the discussion above, it is reasonable to conclude that the difference of the combustion efficiency between the flight and facility conditions was due to the difference in the degree of the chemical reaction.

It is noted that the sizable difference in the combustion pressure-rise between the flight and facility conditions appeared not only with Sc_T=0.3 but also with Sc_T=0.9 although the pressure-rise with Sc_T=0.9 was smaller than that with Sc_T=0.3 because the fuel-air mixing due to the turbulent diffusion was weaker. Further investigation is undergoing.

5. Conclusion

JAXA has initiated the five years research program to clarifying the facility dependence in research and development of hypersonic air-breathing propulsion systems and to develop the numerical tool to predict the actual flight data from the ground test data. The final goal of the project is set to conduct the flight experiment of the supersonic combustion and validate the prediction tools with the real flight data. In this study, to obtain design guidelines for the internal flow-path geometry of the supersonic combustor model mounted on the flight test vehicle, the influence of the difference in the composition of the engine inflow between the flight and facility conditions on the combustion process was examined by both the one-dimensional analysis and the 3D-CFD. The design requirement for the flow-path geometry was to maximize the impact of differences in the inflow composition on combustion and produce sizable differences that can be detected by the wall pressure measurement.

In the one-dimensional analysis, the outline of the combustor shape and the fuel injection condition were assessed. It was shown that, to obtain sizable difference of the wall pressure distributions due to the heat release delay between the flight and facility conditions, there were appropriate ranges of the fuel equivalence ratio and the expansion angle of the diverging cross-sectional area combustor.

The 3D-CFD using the C_2H_4-air skeletal mechanism examined the influence of difference in the inflow composition between the flight and facility conditions on combustion and evaluated the suitability of the candidate combustor flow-path geometries to the design requirement. As for the facility condition, the direct-connect combustor test configuration was assumed for the present study. One of the notable findings was that, when ethylene was used as the fuel, the combustion gas composition was different between the flight and facility conditions. H_2O production was active in the flight condition while CO_2 production was active in the facility condition. The reason is considered because certain amount of H_2O was contained in the VAH freestream and it made the combustion equilibrium state in the facility condition different from that in the flight condition.

Acknowledgments

This work was supported by Innovative Science and Technology Initiative for Security Grant Number JPJ004596, ATLA, Japan.

References

1) Yatsuyanagi, N., Chinzei, N., Mitani, T., Wakamatsu, Y., Masuya, G., Iwagami, S., Endo, M., and Hanus, G.: Ramjet Engine Test Facility (RJTF) in NAL-KRC, Japan, AIAA Paper 1998-1511, 1998.
2) Tomioka, S., Hiraiwa, T., Kobayashi, M., Izumikawa, M., Kishida, T., and Yamasaki, H.: Vitiation Effects on Scramjet Engine Performance in Mach 6 Flight Conditions, *J. Propulsion and Power*, **23** (2007), pp. 789–796.
3) Tani, K., Onodera, T., Kato, K., and Takegoshi, M.: Flight Experiment for the Validation of New Methodology to Compensate the Wind Tunnel Contamination Problem, 32nd International Symposium on Space Technology and Science, Fukui, Japan, 2019-m-11, 2019.
4) Hashimoto, A., Murakami, K., Aoyama, T., Ishiko, K., Hishida, M., Sakashita, M., and Lahur, P.: Toward the Fastest Unstructured CFD Code 'FaSTAR', AIAA Paper 2012-1075, 2012.
5) Billig, F. S.: Research on Supersonic Combustion, *J. Propulsion and Power*, **9** (1993), pp. 499–514.
6) Zambon, A. C. and Chelliah, H. K.: Explicit reduced reaction models for ignition, flame propagation, and extinction of C_2H_4/CH_4/H_2 and air systems, *Combustion and Flame*, **150** (2007), pp. 71–91.
7) Radhakrishnan, K. and Bittker, D. A.: LSENS, A General Chemical Kinetic and Sensitivity Analysis Code for Homogeneous Gas-Phase Reactions - II. Code Description and Usage, NASA RP-1329, 1994.
8) Kitamura, K., Fujimoto, K., Kuzuu, K., Shima, E., and Wang, Z.J.: Validation of Arbitrary Unstructured CFD Code for Aerodynamic Analyses, *Trans. Japan Soc. Aeronaut. Space Sci.*, **53** (2011), pp. 311–319.
9) Takahashi, M., Nojima, K., Kodera, M., Shimizu, T., Aono, J., and Munakata, T.: Numerical Simulation of Ethylene-fueled Scramjet Combustor Flow by Using LS-FLOW Solver (Comparison of the Combustion Gas Composition), Proceedings of the 50th Fluid Dynamics Conference / the 36th Aerospace Numerical Simulation Symposium, Miyazaki, Japan, 3C11, 2018, also JAXA-SP-18-005, 2019, pp. 159–164 (in Japanese).
10) Jackson, K. R. and Gruber, M. R.: HIFiRE Flight 2 – A Program Overview, AIAA Paper 2013-0695, 2013.
11) Gruber, M. R., Jackson, K. R., and Liu, J.: Hydrocarbon-Fueled Scramjet Combustor Flowpath Development for Mach 6-8 HIFiRE Flight Experiment (Preprint), AFRL-RZ-WP-TP-2010-2243, 2008.